



Measurement of $\psi(2S)$ meson production in pp collisions at $\sqrt{s} = 7$ TeV

LHCb collaboration[†]

Abstract

The differential cross-section for the inclusive production of $\psi(2S)$ mesons in pp collisions at $\sqrt{s}=7$ TeV has been measured with the LHCb detector. The data sample corresponds to an integrated luminosity of 36 pb^{-1} . The $\psi(2S)$ mesons are reconstructed in the decay channels $\psi(2S) \rightarrow \mu^+ \mu^-$ and $\psi(2S) \rightarrow J/\psi \pi^+ \pi^-$, with the J/ψ meson decaying into two muons. Results are presented both for promptly produced $\psi(2S)$ mesons and for those originating from b -hadron decays. In the kinematic range $p_T(\psi(2S)) \leq 16 \text{ GeV}/c$ and $2 < y(\psi(2S)) \leq 4.5$ we measure

$$\begin{aligned}\sigma_{\text{prompt}}(\psi(2S)) &= 1.44 \pm 0.01 \text{ (stat)} \pm 0.12 \text{ (syst)}_{-0.40}^{+0.20} \text{ (pol)} \text{ } \mu\text{b}, \\ \sigma_b(\psi(2S)) &= 0.25 \pm 0.01 \text{ (stat)} \pm 0.02 \text{ (syst)} \text{ } \mu\text{b},\end{aligned}$$

where the last uncertainty on the prompt cross-section is due to the unknown $\psi(2S)$ polarization. Recent QCD calculations are found to be in good agreement with our measurements. Combining the present result with the LHCb J/ψ measurements we determine the inclusive branching fraction

$$\mathcal{B}(b \rightarrow \psi(2S)X) = (2.73 \pm 0.06 \text{ (stat)} \pm 0.16 \text{ (syst)} \pm 0.24 \text{ (BF)}) \times 10^{-3},$$

where the last uncertainty is due to the $\mathcal{B}(b \rightarrow J/\psi X)$, $\mathcal{B}(J/\psi \rightarrow \mu^+ \mu^-)$ and $\mathcal{B}(\psi(2S) \rightarrow e^+ e^-)$ branching fraction uncertainties.

All above results are corrected by an erratum included as an appendix.

Published in Eur. Phys. J. C 72 (2012) 2100; Eur. Phys. J. C 80 (2020) 49

© 2020 CERN for the benefit of the LHCb collaboration. CC-BY-4.0 licence.

[†]Authors are listed at the end of this paper.

1 Introduction

Since its discovery, heavy quarkonium has been one of the most important test laboratories for the development of QCD at the border between the perturbative and non-perturbative regimes, resulting in the formulation of the nonrelativistic QCD (NRQCD) factorisation formalism [1, 2]. However, prompt production studies carried out at the Tevatron collider in the early 1990s [3] made clear that NRQCD calculations, based on the leading-order (LO) colour-singlet model (CSM), failed to describe the absolute value and the transverse momentum (p_T) dependence of the charmonium production cross-section and polarization data. Subsequently, the inclusion of colour-octet amplitudes in the NRQCD model has reduced the discrepancy between theory and experiment, albeit at the price of tuning *ad hoc* some matrix elements [2]. On the other hand, recent computations of the next-to-leading-order (NLO) and next-to-next-to-leading-order (NNLO) terms in the CSM yielded predictions in better agreement with experimental data, thus resurrecting interest in the colour-singlet framework. Other models have been proposed and it is important to test them in the LHC energy regime [4, 5].

Heavy quarkonium is also produced from b -hadron decays. It can be distinguished from promptly produced quarkonium exploiting its finite decay time. QCD predictions are based on the Fixed-Order-Next-to-Leading-Log (FONLL) approximation for the $b\bar{b}$ production cross-section. The FONLL approach improves NLO results by resumming p_T logarithms up to the next-to-leading order [6, 7].

To allow a comparison with theory, promptly produced quarkonia should be separated from those coming from b -hadron decays and from those cascading from higher mass states (feed-down). The latter contribution strongly affects J/ψ production and complicates the interpretation of prompt J/ψ data. On the other hand, $\psi(2S)$ charmonium has no appreciable feed-down from higher mass states and therefore the results can be directly compared with the theoretical predictions, making it an ideal laboratory for QCD studies.

This paper presents a measurement of the $\psi(2S)$ meson production cross-section in pp collisions at the centre-of-mass energy $\sqrt{s} = 7$ TeV. The data were collected by the LHCb experiment in 2010 and correspond to an integrated luminosity of 35.9 ± 1.3 pb $^{-1}$. The analysis is similar to that described in Ref. [8] for the J/ψ production studies; in particular, the separation between promptly produced $\psi(2S)$ and those originating from b -hadron decays is based on the reconstructed decay vertex information. Two decay modes of the $\psi(2S)$ meson have been used: $\psi(2S) \rightarrow \mu^+\mu^-$ and $\psi(2S) \rightarrow J/\psi \pi^+\pi^-$ followed by $J/\psi \rightarrow \mu^+\mu^-$. The $J/\psi \pi^+\pi^-$ mode, despite a larger background and a lower reconstruction efficiency, is used to cross-check and average the results, and to extend the accessible phase space. The production of $\psi(2S)$ meson at the LHC has also been studied at the CMS experiment [9].

2 The LHCb detector and data sample

The LHCb detector is a forward spectrometer [10], designed for precision studies of CP violation and rare decays of b - and c -hadrons. Its tracking acceptance covers approximately the pseudorapidity region $2 < \eta < 5$. The detector elements are placed along the beam line of the LHC starting with the vertex detector, a silicon strip device that surrounds the pp interaction region and is positioned at 8 mm from the beams during collisions. It provides

precise measurements of the positions of the primary pp interaction vertices and decay vertices of long-lived hadrons, and contributes to the measurement of particle momenta. Other detectors used for momentum measurement include a large area silicon strip detector located before a dipole magnet of approximately 4 Tm, and a combination of silicon strip detectors and straw drift chambers placed downstream. Two ring imaging Cherenkov detectors are used to identify charged hadrons. Further downstream an electromagnetic calorimeter is used for photon and electron detection, followed by a hadron calorimeter. The muon detection consists of five muon stations equipped with multi-wire proportional chambers, with the exception of the centre of the first station using triple-GEM detectors.

The LHCb trigger system consists of a hardware level, based on information from the calorimeter and the muon systems and designed to reduce the frequency of accepted events to a maximum of 1 MHz, followed by a software level which applies a full event reconstruction. In the first stage of the software trigger a partial event reconstruction is performed. The second stage performs a full event reconstruction to further enhance the signal purity.

The analysis uses events selected by single muon or dimuon triggers. The hardware trigger requires one muon candidate with a p_T larger than 1.4 GeV/ c or two muon candidates with a p_T larger than 560 MeV/ c and 480 MeV/ c . In the first stage of the software trigger, either of the two following selections is required. The first selection confirms the single muon trigger candidate and applies a harder cut on the muon p_T at 1.8 GeV/ c . The second selection confirms the dimuon trigger candidate by requiring the opposite charge of the two muons and adds a requirement to the dimuon mass to be greater than 2.5 GeV/ c^2 . In the second stage of the software trigger, two selections are used for the $\psi(2S) \rightarrow \mu^+\mu^-$ mode. The first tightens the requirement on the dimuon mass to be greater than 2.9 GeV/ c^2 and it applies to the first 8 pb $^{-1}$ of the data sample. Since this selection was subsequently prescaled by a factor five, for the largest fraction of the remaining data (28 pb $^{-1}$) a different selection is used, which in addition requires a good quality primary vertex and tracks for the dimuon system. For the $J/\psi \pi^+\pi^-$ mode only one selection is used which requires the combined dimuon mass to be in a ± 120 MeV/ c^2 mass window around the nominal J/ψ mass. To avoid that a few events with high occupancy dominate the software trigger CPU time, a set of global event cuts is applied on the hit multiplicity of each subdetector used by the pattern recognition algorithms, effectively rejecting events with a large number of pile-up interactions.

The simulation samples used for this analysis are based on the PYTHIA 6.4 generator [11] configured with the parameters detailed in Ref. [12]. The prompt charmonium production processes activated in PYTHIA are those from the leading-order colour-singlet and colour-octet mechanisms. Their implementation and the parameters used are described in detail in Ref. [13]. The EVTGEN package [14] is used to generate hadron decays and the GEANT4 package [15] for the detector simulation. The QED radiative corrections to the decays are generated using the PHOTOS package [16].

3 Signal yield

The two modes, $\psi(2S) \rightarrow \mu^+\mu^-$ and $\psi(2S) \rightarrow J/\psi \pi^+\pi^-$, have different decay and background characteristics, therefore dedicated selection criteria have been adopted. The optimisation of the cuts has been performed using the simulation. A common requirement

is that the tracks, reconstructed in the full tracking system and passing the trigger requirements, must be of good quality ($\chi^2/\text{ndf} < 4$, where ndf is the number of degrees of freedom) and share the same vertex with fit probability $P(\chi^2) > 0.5\%$ ($\psi(2S) \rightarrow \mu^+\mu^-$) and $P(\chi^2) > 5\%$ ($\psi(2S) \rightarrow J/\psi\pi^+\pi^-$). A cut $p_T > 1.2\text{ GeV}/c$ is applied for the muons from the $\psi(2S) \rightarrow \mu^+\mu^-$ decay. For muons from $J/\psi(\mu^+\mu^-)\pi^+\pi^-$ we require a momentum larger than $8\text{ GeV}/c$ and $p_T > 0.7\text{ GeV}/c$. Finally the rapidity of the reconstructed $\psi(2S)$ is required to satisfy the requirement $2 < y \leq 4.5$.

The $\psi(2S) \rightarrow \mu^+\mu^-$ invariant mass spectrum for all selected candidates is shown in Fig. 1(a). The fitting function is a Crystal Ball [17] describing the signal plus an exponential function for the background. In total 90600 ± 690 signal candidates are found in the p_T range $0\text{--}12\text{ GeV}/c$. The mass resolution is $16.01 \pm 0.12\text{ MeV}/c^2$ and the Crystal Ball parameters that account for the radiative tail are obtained from the simulation.

For the $\psi(2S) \rightarrow J/\psi(\mu^+\mu^-)\pi^+\pi^-$ decay, both pions are required to have $p_T > 0.3\text{ GeV}/c$ and the sum of the two-pion transverse momenta is required to be larger than $0.8\text{ GeV}/c$. The quantity $Q = M(J/\psi\pi^+\pi^-) - M(\pi^+\pi^-) - M(\mu^+\mu^-)$ is required to be $\leq 200\text{ MeV}/c^2$ and to improve the mass resolution the dimuon invariant mass $M_{\mu^+\mu^-}$ is constrained in the fit to the nominal J/ψ mass value [18]. Finally, both J/ψ and $\psi(2S)$ candidates must have $p_T > 2\text{ GeV}/c$. The invariant mass spectrum is shown in Fig. 1(b) for all selected candidates. For this decay mode the peak is described by the sum of two Crystal Ball functions for the signal plus an exponential function for the background. The number of signal candidates is 12300 ± 200 , the mass resolution is $2.10 \pm 0.07\text{ MeV}/c^2$, and the Crystal Ball tail parameters are fixed to the values obtained from the simulation.

The fits are repeated in each $\psi(2S)$ p_T bin to obtain the number of signal and background candidates for both decays.

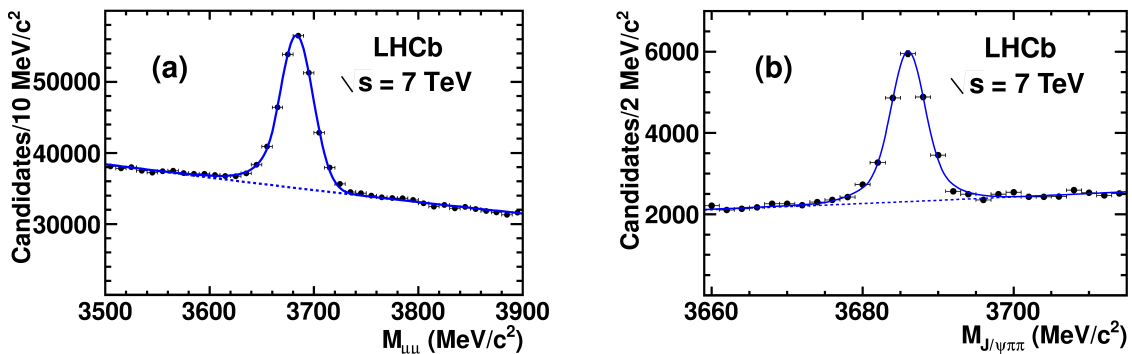


Figure 1: Invariant mass distribution for all $\psi(2S)$ candidates passing the selection cuts for the $\mu^+\mu^-$ decay (a) and the $J/\psi(\mu^+\mu^-)\pi^+\pi^-$ decay (b).

4 Cross-section measurement

The differential cross-section for the inclusive $\psi(2S)$ meson production is computed from

$$\frac{d\sigma}{dp_T}(p_T) = \frac{N_{\text{sig}}(p_T)}{\mathcal{L} \epsilon_{\text{tot}}(p_T) \mathcal{B} \Delta p_T} \quad (1)$$

where $d\sigma/dp_T$ is the average cross-section in the given p_T bin, integrated over the rapidity range $2 < y \leq 4.5$, $N_{\text{sig}}(p_T)$ is the number of signal candidates determined from the mass fit for the decay under study, $\epsilon_{\text{tot}}(p_T)$ is the total detection efficiency including acceptance and trigger effects, \mathcal{B} denotes the relevant branching fraction and Δp_T is the bin size. All branching fractions are taken from Ref. [18]: $\mathcal{B}(\psi(2S) \rightarrow e^+e^-) = (7.72 \pm 0.17) \times 10^{-3}$, $\mathcal{B}(\psi(2S) \rightarrow J/\psi \pi^+\pi^-) = (33.6 \pm 0.4) \times 10^{-2}$ and $\mathcal{B}(J/\psi \rightarrow \mu^+\mu^-) = (5.93 \pm 0.06) \times 10^{-2}$. Assuming lepton universality, we use the dielectron branching fraction $\mathcal{B}(\psi(2S) \rightarrow e^+e^-)$ in Eq. (1), since $\mathcal{B}(\psi(2S) \rightarrow \mu^+\mu^-)$ is less precisely known. \mathcal{L} is the integrated luminosity, which is calibrated using both Van der Meer scans [19,20] and a beam-profile method [21]. A detailed description of the two methods is given in Ref. [22]. The knowledge of the absolute luminosity scale is used to calibrate the number of tracks in the vertex detector, which is found to be stable throughout the data taking period and can therefore be used to monitor the instantaneous luminosity of the entire data sample. The integrated luminosity of the data sample used in this analysis is determined to be 35.9 pb^{-1} .

The total efficiency, $\epsilon_{\text{tot}}(p_T)$, is a product of three contributions: the geometrical acceptance, the combined detection, reconstruction and selection efficiency, and the trigger efficiency. Each contribution has been determined using simulated events for the two decay channels. In order to evaluate the trigger efficiency, the trigger selection algorithms used during data taking are applied to the simulation.

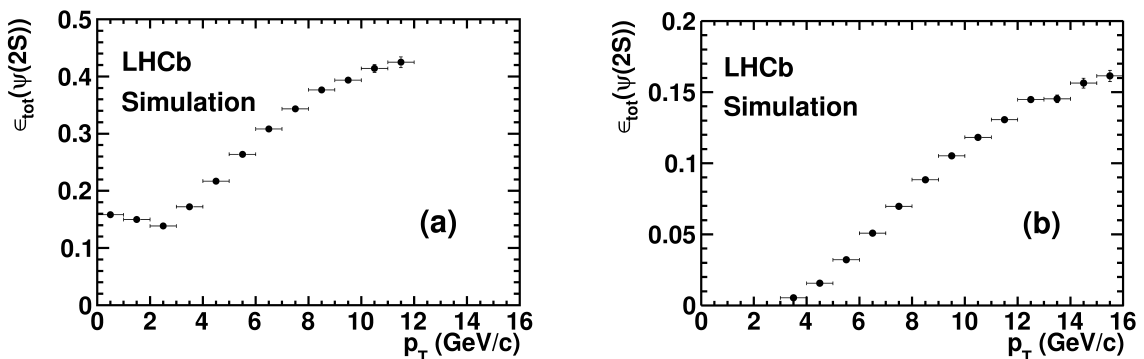


Figure 2: Total efficiency *vs.* p_T computed from simulation for unpolarized $\psi(2S)$ mesons for $\psi(2S) \rightarrow \mu^+\mu^-$ (a) and $\psi(2S) \rightarrow J/\psi(\mu^+\mu^-)\pi^+\pi^-$ (b).

The total efficiency *vs.* p_T for the two channels, assuming the $\psi(2S)$ meson unpolarized, is shown in Fig. 2. Extensive studies on dimuon decays of prompt J/ψ [8], $\psi(2S)$ and Υ [23] mesons have shown that the total efficiency in the LHCb detector depends strongly on the initial polarization state of the vector meson. This effect is absent for $\psi(2S)$ mesons coming from b -hadron decays. In fact for these events the natural polarization axis is the $\psi(2S)$ meson flight direction in the b -hadron rest frame, while the $\psi(2S)$ meson appears unpolarized along its flight direction in the laboratory. Simulations [8] and measurements from CDF [24] confirm this. We do not measure the $\psi(2S)$ meson polarization but we assign a systematic uncertainty to the unpolarized efficiencies in the case of prompt production. Events are generated with polarizations corresponding to the two extreme cases of fully transverse or fully longitudinal polarization and the efficiency is re-evaluated. The difference between these results and those with the unpolarized sample is taken as an

estimate of the systematic uncertainty.

A similar effect exists for the J/ψ meson emitted in the $\psi(2S) \rightarrow J/\psi(\mu^+\mu^-)\pi^+\pi^-$ decay. However, in this case, the $\psi(2S)$ meson polarization is fully transferred to the J/ψ meson since, as measured by the BES collaboration [25], the two pions are predominantly in the S -wave configuration¹ and the dipion- J/ψ system is also in a S -wave configuration. This has been verified with data and is correctly reproduced by the simulation. Therefore the systematics due to polarization are fully correlated between the two channels and we use the systematic uncertainties computed for $\psi(2S) \rightarrow \mu^+\mu^-$ also for the $\psi(2S) \rightarrow J/\psi\pi^+\pi^-$ decay.

In order to separate prompt $\psi(2S)$ mesons from those produced in b -hadron decays, we use the pseudo-decay-time variable defined as $t = d_z(M/p_z)$, where d_z is the separation along the beam axis between the $\psi(2S)$ decay vertex and the primary vertex, M is the nominal mass of the $\psi(2S)$ and p_z is the component of its momentum along the beam axis. In case of multiple primary vertices reconstructed in the same event, that which minimises $|d_z|$ has been chosen. The prompt component is distributed as a Gaussian function around $t = 0$, with width corresponding to the experimental resolution, while for the $\psi(2S)$ from b -hadron decays the t variable is distributed according to an approximately exponential decay law, smeared in the fit with the experimental resolution. The choice of taking the primary vertex which minimises $|d_z|$ could in principle introduce a background component in the pseudo-decay-time distribution arising from the association of the $\psi(2S)$ vertex to a wrong primary vertex. The effect of such background is found to be of the order of 0.5% in the region around $t = 0$ and has been neglected. The function used to fit the t distribution in each p_T bin is

$$F(t; f_p, \sigma, \tau_b) = N_{\text{sig}} \left[f_p \delta(t) + (1 - f_p) \theta(t) \frac{e^{-\frac{t}{\tau_b}}}{\tau_b} \right] \otimes \frac{e^{-\frac{1}{2}(\frac{t}{\sigma})^2}}{\sqrt{2\pi}\sigma} + N_{\text{bkg}} f_{\text{bkg}}(t; \Theta) \quad (2)$$

where N_{sig} and N_{bkg} are respectively the numbers of signal and background candidates obtained from the mass fit. The fit parameters are the prompt fraction, f_p , the standard deviation of the Gaussian resolution function, σ , and the lifetime describing the long-lived component of $\psi(2S)$ mesons coming from b -hadron decays, τ_b . In principle, all fit parameters are dependent on p_T . The function $f_{\text{bkg}}(t; \Theta)$ models the background component in the distribution and is defined as the sum of a δ function and a Gaussian function for the prompt background, plus two exponential functions for the positive tail and one exponential function for the negative tail, all convolved with a Gaussian function to account for the detector resolution. The array of parameters Θ is determined from a fit to the t distribution of the events in the mass sidebands.

As an example, the pseudo-decay-time distributions for $\psi(2S) \rightarrow \mu^+\mu^-$ and $\psi(2S) \rightarrow J/\psi\pi^+\pi^-$ in the p_T range $4 < p_T \leq 5 \text{ GeV}/c$ are presented in Fig. 3. The contributions of background and prompt $\psi(2S)$ mesons are also shown. The values of the prompt fraction, f_p vs. p_T in the rapidity range $2 < y \leq 4.5$, obtained for the $\mu^+\mu^-$ and the $J/\psi\pi^+\pi^-$ modes, are in good agreement as shown in Fig. 4.

¹The small fraction of D -wave measured in Ref. [25] has a negligible impact on our conclusion.

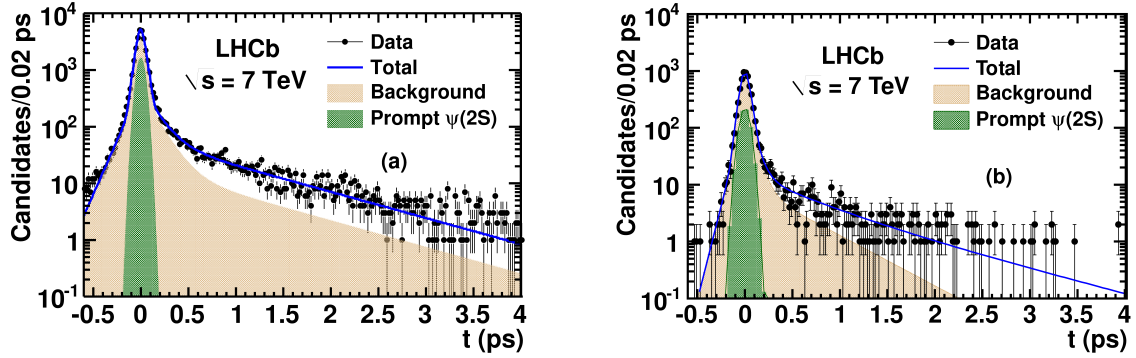


Figure 3: Pseudo-decay-time distribution for $\psi(2S) \rightarrow \mu^+\mu^-$ (a) and $\psi(2S) \rightarrow J/\psi\pi^+\pi^-$ (b) in the p_T range $4 < p_T \leq 5$ GeV/c, showing the background and prompt contributions. **This figure is updated in the Erratum (Appendix A)**

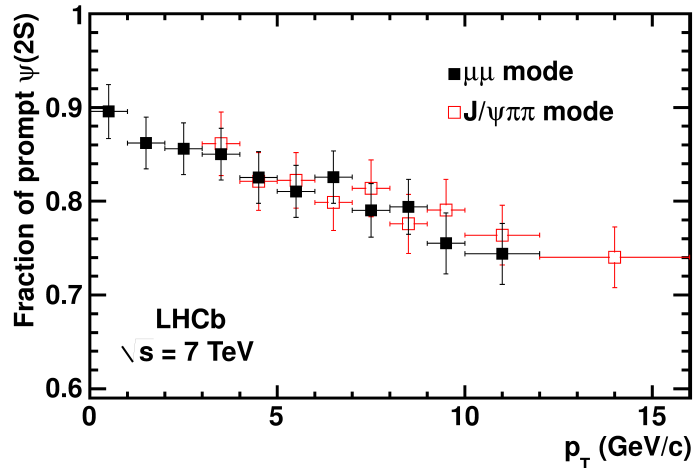


Figure 4: Fraction of prompt $\psi(2S)$ as a function of p_T for the $\mu^+\mu^-$ mode (solid squares) and the $J/\psi\pi^+\pi^-$ mode (open squares). Error bars include the statistical uncertainties and the systematic uncertainties due to the fitting procedure. **This figure is updated in the Erratum (Appendix A).**

5 Systematic uncertainties on the cross-section measurement

A variety of sources of systematic uncertainties affecting the cross-section measurement were taken into account and are summarised in Table 1.

A thorough analysis of the luminosity scans yields consistent results for the absolute luminosity scale with a precision of 3.5% [22], this value being assigned as a systematic uncertainty. The statistical uncertainties from the finite number of simulated events on the efficiencies are included as a source of systematic uncertainty; this uncertainty varies from 0.4 to 2.2% for the $\mu^+\mu^-$ mode and from 0.6 to 1% for the $J/\psi\pi^+\pi^-$ mode. In addition,

Table 1: Systematic uncertainties included in the measurement of the cross-section. Uncertainties labelled with a are correlated between the $\mu^+\mu^-$ and $J/\psi\pi^+\pi^-$ mode, while b indicates a correlation between $\psi(2S) \rightarrow \mu^+\mu^-$ and the $J/\psi \rightarrow \mu^+\mu^-$ uncertainties [8].

Uncertainty source	$\mu^+\mu^-$ (%)	$J/\psi\pi^+\pi^-$ (%)
Luminosity ^{a,b}	3.5	3.5
Size of simulation sample	0.4–2.2	0.6–1.0
Trigger efficiency ^{a}	1–8	1–7
Global event cuts ^{a,b}	2.1	2.1
Muon identification ^{a,b}	1.1	1.1
Hadron identification	–	0.5
Track χ^2 ^{a,b}	1	2
Tracking efficiency ^{a}	3.5	7.3
Vertex fit ^{b}	0.8	1.3
Unknown polarization ^{a}	15–26	15–26
Mass fit function	1.1	0.5
Pseudo-decay-time fits	2.7	2.7
$\mathcal{B}(\psi(2S) \rightarrow e^+e^-)$	2.2	–
$\mathcal{B}(\psi(2S) \rightarrow J/\psi\pi^+\pi^-)$	–	1.2
$\mathcal{B}(J/\psi \rightarrow \mu^+\mu^-)$	–	1.0

we assign a systematic uncertainty in order to account for the difference between the trigger efficiency evaluated on data by means of an unbiased $\mu^+\mu^-$ sample, and the trigger efficiency computed from the simulation. This results in a bin-dependent uncertainty up to 8% for the $\mu^+\mu^-$ mode and up to 7% for the $J/\psi\pi^+\pi^-$ mode. This uncertainty is fully correlated between the two decay modes in the overlapping p_T region. Finally, the statistical uncertainty on the global event cuts efficiency (2.1% for both modes) is taken as an additional systematic uncertainty [8].

To assess possible systematic differences in the acceptance between data and simulation for the $J/\psi\pi^+\pi^-$ mode, we have studied the dipion mass distribution. The LHCb simulation is based on the Voloshin-Zakharov model [26] which uses a single phenomenological parameter λ

$$\frac{d\sigma}{dm_{\pi\pi}} \propto \Phi(m_{\pi\pi}) [m_{\pi\pi}^2 - \lambda m_\pi^2]^2, \quad (3)$$

where $\Phi(m_{\pi\pi})$ is a phase space factor (see e.g. Ref. [25]) and in the simulation $\lambda = 4$ is assumed. The dipion mass distribution obtained from the data is shown in Fig. 5. We obtain $\lambda = 4.46 \pm 0.07(\text{stat}) \pm 0.18(\text{syst})$, from which we estimate a negligible systematic effect on the acceptance (0.25%). Our result is also in good agreement with the BES value $\lambda = 4.36 \pm 0.06(\text{stat}) \pm 0.17(\text{syst})$ [25].

To cross-check and assign a systematic uncertainty to the determination of the muon identification efficiency from simulation, the single track muon identification efficiency has been measured on data using a tag-and-probe method [27]. This gives a correction factor for the dimuon of 1.025 ± 0.011 , which we apply to the simulation efficiencies. The 1.1% uncertainty on the correction factor is used as systematic uncertainty. The efficiency of the selection requirement on the dipion identification has been studied on data and simulation

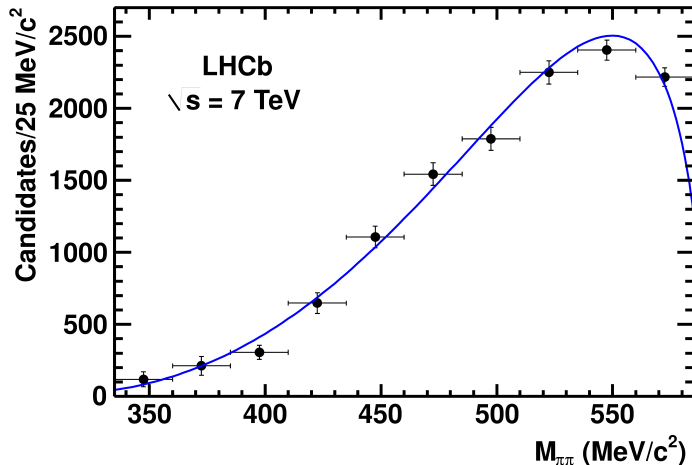


Figure 5: Dipion mass spectrum for the $\psi(2S) \rightarrow J/\psi \pi^+ \pi^-$ decay. The curve shows the result of the fit with Eq. (3) corrected for the acceptance.

and a difference of 1% has been measured between the two. Therefore, the simulation efficiencies are corrected for this difference and an additional systematic uncertainty of 0.5% is included.

The $\psi(2S)$ selection also includes a requirement on the track fit quality. The relative difference between the efficiency of this requirement in simulation and data is taken as a systematic uncertainty, resulting in an uncertainty of 0.5% per track. Tracking studies show that the ratio of the track-finding efficiencies between data and simulation is 1.09 for the $\mu^+ \mu^-$ mode and 1.06 for the $J/\psi \pi^+ \pi^-$ mode, with an uncertainty of 3.5% and 7.3% respectively; the simulation efficiencies are corrected accordingly and the corresponding systematic uncertainties are included.

For the requirement on the secondary vertex fit quality, a relative difference of 1.6% for the $\mu^+ \mu^-$ mode and 2.6% for the $J/\psi \pi^+ \pi^-$ mode has been measured between data and simulation. The simulation efficiency is therefore corrected for this difference and a corresponding systematic uncertainty of 0.8% ($\mu^+ \mu^-$) and 1.3% ($J/\psi \pi^+ \pi^-$) is assigned.

The systematic uncertainty due to the unknown polarization is computed as discussed in Section 4. The study done for the two extreme polarization hypotheses gives an average systematic uncertainty between 15% and 26% for both modes, relative to the hypothesis of zero polarization, depending on the p_T bin. These errors are fully correlated between the two decay modes and strongly asymmetric since the variations of the efficiency are of different magnitude for transverse and longitudinal polarizations.

A systematic uncertainty from the fitting procedure has been estimated from the relative difference between the overall number of signal $\psi(2S)$ and the number of signal candidates obtained by summing the results of the fits in the individual p_T bins. A total systematic uncertainty of 1.1% for the $\mu^+ \mu^-$ mode and 0.5% for the $J/\psi \pi^+ \pi^-$ mode is assigned.

Finally, to evaluate the systematic uncertainty on the prompt fraction from the $\psi(2S)$ pseudo-decay-time fit we recompute f_p with τ_b (see Eq. (2)) fixed to the largest and smallest value obtained in the p_T -bin fits. The relative variation is at most 2.7% and this

value is assigned as a systematic uncertainty on f_p .

6 Cross-section results

The differential cross-sections for prompt $\psi(2S)$ and $\psi(2S)$ mesons from b -hadron decays are shown in Fig. 6, where we compare the results obtained for the $\psi(2S) \rightarrow \mu^+\mu^-$ and $\psi(2S) \rightarrow J/\psi \pi^+\pi^-$ channels separately for the prompt and b -hadron decay components.

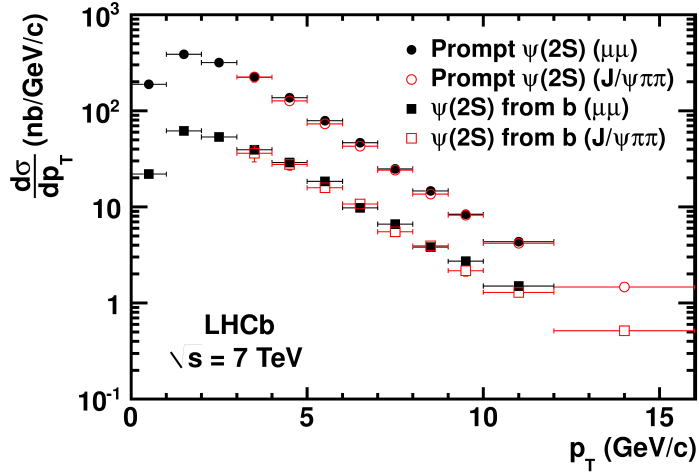


Figure 6: Comparison of the differential cross-sections measured for prompt $\psi(2S)$ (circles) and for $\psi(2S)$ from b -hadron decay (squares) in the $\psi(2S) \rightarrow \mu^+\mu^-$ (solid symbols) and $\psi(2S) \rightarrow J/\psi \pi^+\pi^-$ (open symbols) modes. Only the uncorrelated uncertainties are shown. **This figure is obsolete. Corrected cross sections are found in Figs. 7 and 8 in the Erratum.**

The values for the two cross-sections estimated using the different decay modes are consistent within 0.5σ . A weighted average of the two measurements is performed to extract the final result listed in Table 2.

The differential cross-section for promptly produced $\psi(2S)$ mesons, along with a comparison with some recent theory predictions [28–31] tuned to the LHCb acceptance, is shown in Fig. 7. In Ref. [28] and Ref. [29] the differential prompt cross-section has been computed up to NLO terms in nonrelativistic QCD, including colour-singlet and colour-octet contributions. In Ref. [30,31] the prompt cross-section has been evaluated in a colour-singlet framework, including up to the dominant α_s^5 NNLO terms. Experimentally the large- p_T tail behaves like $p_T^{-\beta}$ with $\beta = 4.2 \pm 0.6$ and is rather well reproduced, especially in the colour-octet models.

The differential cross-section for $\psi(2S)$ produced in b -hadron decays and the comparison with a recent theory prediction [32] based on the FONLL approach [6, 7] are presented in Fig. 8. The theoretical prediction of Ref. [32] uses as input the $b \rightarrow \psi(2S)X$ branching fraction obtained in the following section. Experimentally the $\psi(2S)$ mesons resulting from b -hadron decay have a slightly harder p_T spectrum than those produced promptly: $\beta = 3.6 \pm 0.5$. By integrating the differential cross-section for prompt $\psi(2S)$ and $\psi(2S)$

Table 2: Cross-section values for prompt $\psi(2S)$ and $\psi(2S)$ from b -hadrons in different p_T bins and in the range $2 < y \leq 4.5$, evaluated as the weighted average of the $\mu^+\mu^-$ and $J/\psi\pi^+\pi^-$ channels. The first error is statistical, the second error is systematic, and the last asymmetric uncertainty is due to the unknown polarization of the prompt $\psi(2S)$ meson. **This table is updated in the Erratum.**

p_T [GeV/ c]	$\frac{d\sigma_{\text{prompt}}}{dp_T}$ [$\frac{\text{nb}}{\text{GeV}/c}$]	$\frac{d\sigma_b}{dp_T}$ [$\frac{\text{nb}}{\text{GeV}/c}$]
0–1	$188 \pm 6 \pm 18_{-67}^{+32}$	$22 \pm 2 \pm 2$
1–2	$387 \pm 8 \pm 37_{-119}^{+60}$	$62 \pm 3 \pm 6$
2–3	$317 \pm 7 \pm 26_{-88}^{+44}$	$53 \pm 2 \pm 4$
3–4	$224 \pm 6 \pm 24_{-53}^{+27}$	$39 \pm 2 \pm 4$
4–5	$135 \pm 4 \pm 13_{-30}^{+16}$	$29 \pm 1 \pm 3$
5–6	$77 \pm 2 \pm 7_{-18}^{+9}$	$18 \pm 1 \pm 2$
6–7	$46 \pm 1 \pm 4_{-10}^{+5}$	$10 \pm 1 \pm 1$
7–8	$25 \pm 1 \pm 2_{-6}^{+3}$	$6.3 \pm 0.4 \pm 0.5$
8–9	$14 \pm 1 \pm 1_{-3}^{+2}$	$3.9 \pm 0.3 \pm 0.3$
9–10	$8.3 \pm 0.4 \pm 0.7_{-1.7}^{+0.9}$	$2.5 \pm 0.2 \pm 0.2$
10–12	$4.3 \pm 0.3 \pm 0.4_{-0.9}^{+0.5}$	$1.4 \pm 0.1 \pm 0.1$
12–16	$1.5 \pm 0.1 \pm 0.2_{-0.3}^{+0.2}$	$0.51 \pm 0.04 \pm 0.06$

from b -hadrons in the range $2 < y \leq 4.5$ and $p_T \leq 16 \text{ GeV}/c$, we obtain

$$\begin{aligned}\sigma_{\text{prompt}}(\psi(2S)) &= 1.44 \pm 0.01 \text{ (stat)} \pm 0.12 \text{ (syst)}_{-0.40}^{+0.20} \text{ (pol)} \mu\text{b}, \\ \sigma_b(\psi(2S)) &= 0.25 \pm 0.01 \text{ (stat)} \pm 0.02 \text{ (syst)} \mu\text{b},\end{aligned}$$

where the systematic uncertainty includes all the sources listed in Table 1, except for the polarization, while the last asymmetric uncertainty is due to the effect of the unknown $\psi(2S)$ polarization and applies only to the prompt component.

7 Inclusive $b \rightarrow \psi(2S)X$ branching fraction measurement

The inclusive branching fraction for a b -hadron decaying to $\psi(2S)$ is presently known with 50% precision: $\mathcal{B}(b \rightarrow \psi(2S)X) = (4.8 \pm 2.4) \times 10^{-3}$ [18]. Combining the present result for $\sigma_b(\psi(2S))$ with the previous measurement of $\sigma_b(J/\psi)$ [8] we can obtain an improved value of the aforementioned branching fraction. To achieve this, it is necessary to extrapolate the two measurements to the full phase space. The extrapolation factors for the two decays have been determined using the LHCb simulation [12] and they have been found to be $\alpha_{4\pi}(J/\psi)=5.88$ [8] and $\alpha_{4\pi}(\psi(2S))=5.48$. Most of the theoretical uncertainties are expected to cancel in the ratio of the two factors $\xi = \alpha_{4\pi}(\psi(2S))/\alpha_{4\pi}(J/\psi) = 0.932$,

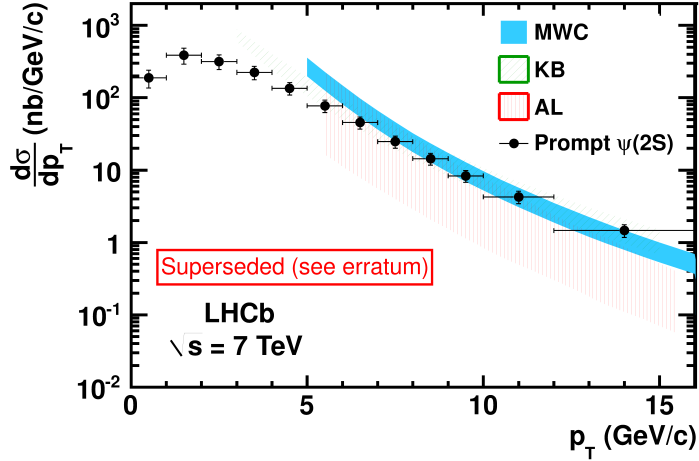


Figure 7: Differential production cross-section *vs.* p_T for prompt $\psi(2S)$. The predictions of three nonrelativistic QCD models are also shown for comparison. MWC [28] and KB [29] are NLO calculations including colour-singlet and colour-octet contributions. AL [30,31] is a colour-singlet model including the dominant NNLO terms. **This figure is updated in the Erratum.**

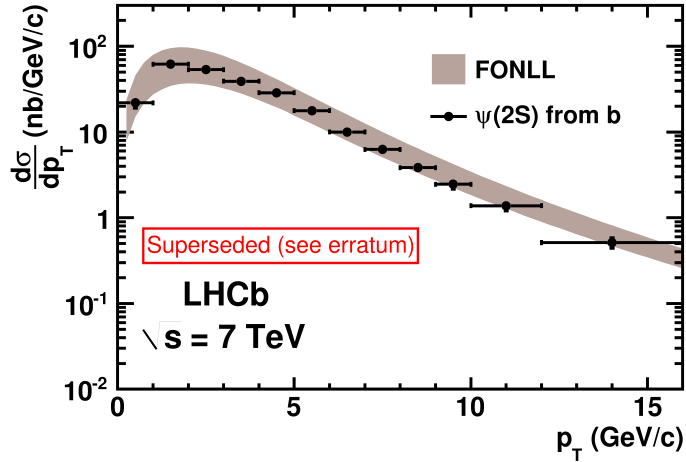


Figure 8: Differential production cross-section *vs.* p_T for $\psi(2S)$ from b -hadrons. The shaded band is the prediction of a FONLL calculation [6, 7, 32]. **This figure is updated in the Erratum.**

which is used in Eq. (4). A systematic uncertainty of 3.4% is estimated for this correction and included in the final result below. Therefore

$$\frac{\mathcal{B}(b \rightarrow \psi(2S)X)}{\mathcal{B}(b \rightarrow J/\psi X)} = \xi \frac{\sigma_b(\psi(2S))}{\sigma_b(J/\psi)}. \quad (4)$$

For $\sigma_b(J/\psi)$ we rescale the value in [8] for the new determination of the integrated luminosity ($\mathcal{L} = 5.49 \pm 0.19 \text{ pb}^{-1}$). For $\sigma_b(\psi(2S))$ we use only the data from the $\psi(2S) \rightarrow \mu^+\mu^-$ mode to cancel most of the systematic uncertainties in the ratio. Effects

due to polarization are negligible for mesons resulting from b -hadron decay. We obtain

$$\frac{\mathcal{B}(b \rightarrow \psi(2S)X)}{\mathcal{B}(b \rightarrow J/\psi X)} = 0.235 \pm 0.005 \text{ (stat)} \pm 0.015 \text{ (syst)},$$

where the correlated uncertainties (Table 1) between the two cross-sections are excluded. By inserting the value $\mathcal{B}(b \rightarrow J/\psi X) = (1.16 \pm 0.10) \times 10^{-2}$ [18] we get

$$\mathcal{B}(b \rightarrow \psi(2S)X) = (2.73 \pm 0.06 \text{ (stat)} \pm 0.16 \text{ (syst)} \pm 0.24 \text{ (BF)}) \times 10^{-3},$$

where the last uncertainty originates from the uncertainty of the branching fractions $\mathcal{B}(b \rightarrow J/\psi X)$, $\mathcal{B}(\psi(2S) \rightarrow e^+e^-)$ and $\mathcal{B}(J/\psi \rightarrow \mu^+\mu^-)$.

The ratio of the $\psi(2S) \rightarrow \mu^+\mu^-$ to $J/\psi \rightarrow \mu^+\mu^-$ differential cross-sections is shown *vs.* p_T in Fig. 9 for prompt production (R_p , Fig. 9(a)) and when the vector mesons originate from b -hadron decays (R_b , Fig. 9(b)). Since it is not known if the promptly produced $\psi(2S)$ and J/ψ have similar polarizations [33], we do not assume any correlation of the polarization uncertainties when computing the uncertainties on R_p . The increase of $R_{p(b)}$ with p_T is similar to that measured in the central rapidity region by the CDF [24] and CMS [9] collaborations. **These results are updated by Sec. A.2.**

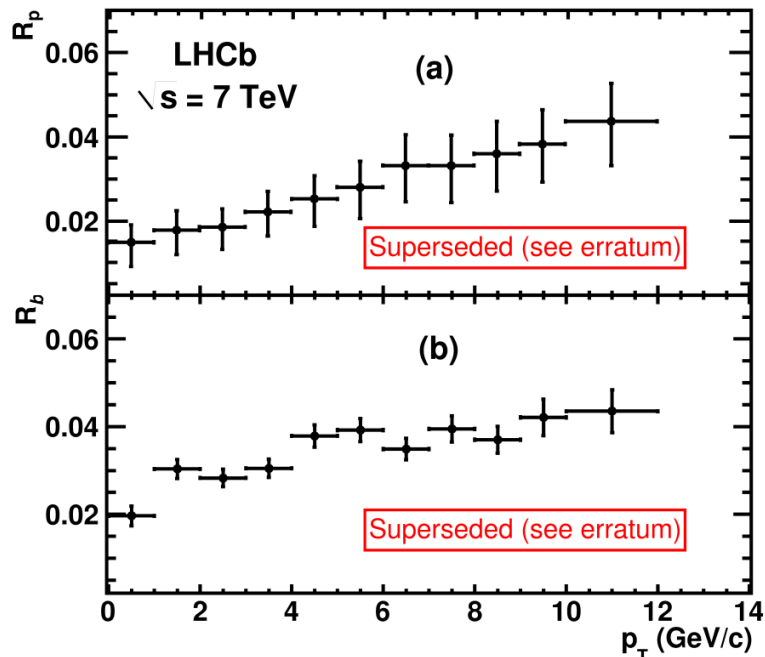


Figure 9: Ratio of $\psi(2S) \rightarrow \mu^+\mu^-$ to $J/\psi \rightarrow \mu^+\mu^-$ cross-sections for prompt production (a) and for b -hadron decay (b), as a function of p_T . **This figure is updated in the Erratum.**

8 Conclusions

We have measured the differential cross-section for the process $pp \rightarrow \psi(2S)X$ at the centre-of-mass energy of 7 TeV, as a function of the transverse momentum in the range

$p_T(\psi(2S)) \leq 16 \text{ GeV}/c$ and $2 < y(\psi(2S)) \leq 4.5$, via the decay modes $\psi(2S) \rightarrow \mu^+\mu^-$ and $\psi(2S) \rightarrow J/\psi \pi^+\pi^-$. The data sample corresponds to about 36 pb^{-1} collected by the LHCb experiment at the LHC. Results from the two decay modes agree. The $\psi(2S)$ prompt cross-section has been separated from the cross-section of $\psi(2S)$ from b -hadrons through the study of the pseudo-decay-time and the two measurements have been averaged. In the above kinematic range we measure

$$\begin{aligned}\sigma_{\text{prompt}}(\psi(2S)) &= 1.44 \pm 0.01 \text{ (stat)} \pm 0.12 \text{ (syst)}_{-0.40}^{+0.20} \text{ (pol)} \text{ } \mu\text{b}, \\ \sigma_b(\psi(2S)) &= 0.25 \pm 0.01 \text{ (stat)} \pm 0.02 \text{ (syst)} \text{ } \mu\text{b}.\end{aligned}$$

The measured $\psi(2S)$ production cross-sections are in good agreement with the results of several recent NRQCD calculations. In addition, we obtain an improved value for the $b \rightarrow \psi(2S)X$ branching fraction by combining the two LHCb production cross-section measurements of the two vector mesons J/ψ and $\psi(2S)$ from b -hadrons. The result,

$$\mathcal{B}(b \rightarrow \psi(2S)X) = (2.73 \pm 0.06 \text{ (stat)} \pm 0.16 \text{ (syst)} \pm 0.24 \text{ (BF)}) \times 10^{-3},$$

is in good agreement with recent results from the CMS collaboration [9] and is a significant improvement over the present PDG average [18].

The results above are corrected by the Erratum in Appendix A.

Acknowledgments

We express our gratitude to our colleagues in the CERN accelerator departments for the excellent performance of the LHC. We thank the technical and administrative staff at CERN and at the LHCb institutes, and acknowledge support from the National Agencies: CAPES, CNPq, FAPERJ and FINEP (Brazil); CERN; NSFC (China); CNRS/IN2P3 (France); BMBF, DFG, HGF and MPG (Germany); SFI (Ireland); INFN (Italy); FOM and NWO (The Netherlands); SCSR (Poland); ANCS (Romania); MinES of Russia and Rosatom (Russia); MICINN, XUNGAL and GENCAT (Spain); SNSF and SER (Switzerland); NAS Ukraine (Ukraine); STFC (United Kingdom); NSF (USA). We also acknowledge the support received from the ERC under FP7 and the Region Auvergne.

We thank B. Kniehl, M. Butenschön and M. Cacciari for providing theoretical predictions of $\psi(2S)$ cross-sections in the LHCb acceptance range.

References

- [1] W. E. Caswell and G. P. Lepage, *Effective lagrangians for bound state problems in QED, QCD, and other field theories*, Phys. Lett. **B167** (1986) 437.
- [2] G. T. Bodwin, E. Braaten, and G. P. Lepage, *Rigorous QCD analysis of inclusive annihilation and production of heavy quarkonium*, Phys. Rev. D **51** (1995) 1125. [Erratum-ibid. D 55 (1997) 5853], [arXiv:hep-ph/9407339](#).
- [3] CDF collaboration, F. Abe *et al.*, *Inclusive J/ψ , $\psi(2S)$, and b -quark production in $\bar{p}p$ collisions at $\sqrt{s} = 1.8$ TeV*, Phys. Rev. Lett. **69** (1992) 3704.
- [4] N. Brambilla *et al.*, *Heavy quarkonium physics*, (2005) [arXiv:hep-ph/0412158v2](#).
- [5] N. Brambilla *et al.*, *Heavy quarkonium: progress, puzzles and opportunities*, (2010) [arXiv:hep-ph/1010.5827v1](#).
- [6] M. Cacciari, M. Greco, P. Nason, *The p_T spectrum in heavy-flavour hadroproduction*, JHEP **9805** (1998) 007.
- [7] M. Cacciari, S. Frixione, M. Mangano, P. Nason and G. Ridolfi, *QCD analysis of first b cross section data at 1.96 TeV*, JHEP **0407** (2004) 033.
- [8] LHCb collaboration, R. Aaij *et al.*, *Measurement of J/ψ production in pp collisions at $\sqrt{s}=7$ TeV*, Eur. Phys. J. C **71** (2011) 1645.
- [9] CMS collaboration, S. Chatrchyan *et al.*, *J/ψ and $\psi(2S)$ production in pp collisions at $\sqrt{s} = 7$ TeV*, JHEP **02** (2011) 11.
- [10] LHCb collaboration, A. A. Alves Jr. *et al.*, *The LHCb detector at the LHC*, JINST **3** (2008) S08005.
- [11] I. Belyaev *et al.*, *Handling of the generation of primary events in GAUSS, the LHCb simulation framework*, Nuclear Science Symposium Conference Record (NSS/MIC) **IEEE** (2010) 1155.
- [12] M. Clemencic *et al.*, *The LHCb simulation application, Gauss: design, evolution and experience*, Journal of Physics: Conference Series **331** (2011), no. 3 032023.
- [13] M. Bargiotti and V. Vagnoni, *Heavy quarkonia sector in PYTHIA 6.324 : tuning, validation and perspectives at LHCb*, CERN-LHCb-2007-042.
- [14] D. J. Lange, *The EvtGen particle decay simulation package*, Nucl. Instrum. Meth. **A462** (2001) 152.
- [15] GEANT4 collaboration, S. Agostinelli *et al.*, *GEANT4: a simulation toolkit*, Nucl. Instrum. Meth. **A506** (2003) 250.
- [16] P. Golonka and Z. Was, *PHOTOS Monte Carlo: a precision tool for QED corrections in Z and W decays*, Eur. Phys. J. C **45** (2006) 97.

- [17] T. Skwarnicki, *A study of the radiative cascade transitions between the Upsilon-prime and Upsilon resonances*. PhD thesis, Institute of Nuclear Physics, Krakow, 1986. DESY-F31-86-02.
- [18] Particle Data Group, K. Nakamura *et al.*, *Review of particle physics*, J. Phys. G37 Journal of Physics G**37** (2010) 075201.
- [19] S. Van der Meer, *Calibration of the effective beam height in the ISR*, CERN report, ISR-PO/68-31, (1968).
- [20] H. Burkhardt and P. Grafström, *Absolute luminosity from machine parameters*, CERN-LHC-PROJECT-Report-1019 (2007).
- [21] M. Ferro-Luzzi, *Proposal for an absolute luminosity determination in colliding beam experiments using vertex detection of beam-gas interactions*, Nucl. Instrum. Meth. A**553** (2005) 388-399.
- [22] LHCb collaboration, R. Aaij *et al.*, *Absolute luminosity measurements with the LHCb detector at the LHC*, JINST **7** (2012) P01010.
- [23] LHCb collaboration, R. Aaij *et al.*, *Measurement of Υ production in pp collisions at $\sqrt{s} = 7$ TeV*, arXiv:hep-ex/1202.6579v1.
- [24] CDF collaboration, T. Aaltonen *et al.*, *Production of $\psi(2S)$ mesons in $p\bar{p}$ collisions at 1.96 TeV*, Phys. Rev. D**80** (2009) 031103.
- [25] BES collaboration, J. Bai *et al.*, *$\pi^+\pi^-J/\psi$ decay distributions*, Phys. Rev. D**62** (2000) 032002.
- [26] M. Voloshin and V. Zakharov, *Measuring quantum-chromodynamic anomalies in hadronic transitions between quarkonium states*, Phys. Rev. Lett. **45**, (1980) 688-691.
- [27] A. Sarti *et al.*, *Calibration strategy and efficiency measurement of the muon identification procedure at LHCb*, LHCb-PUB-2010-002.
- [28] Y.-Q. Ma, K. Wang and K.-T. Chao, *A complete NLO calculation of the J/ψ and ψ' production at hadron colliders*, arXiv:hep-ph/1012.1030.
- [29] B. Kniehl and M. Butenschön, *Reconciling J/ψ production at HERA, RHIC, Tevatron, and LHC with nonrelativistic QCD factorization at next-to-leading order*, Phys. Rev. Lett. **106** (2011) 022003, and private communication.
- [30] P. Artoisenet *et al.*, *Υ production at Fermilab Tevatron and LHC energies*, Phys. Rev. Lett. **101** (2008) 152001.
- [31] J.-P. Lansberg, *On the mechanisms of heavy-quarkonium hadroproduction*, Eur. Phys. J. C**61** (2009) 693.
- [32] M. Cacciari, private communication.
- [33] CDF collaboration, A. Abulencia *et al.*, *Polarizations of J/ψ and $\psi(2S)$ mesons produced in $p\bar{p}$ collisions at $\sqrt{s} = 1.96$ TeV*, Phys. Rev. Lett. **99** (2007) 132001.

A Erratum

This erratum corrects measurements of the prompt and secondary (from- b) $\psi(2S)$ production cross-sections in the forward region in pp collisions at $\sqrt{s} = 7$ TeV. The original measurements, reported in the body of this preprint, were performed using data collected with the LHCb detector in 2010 and were published in Ref. [1]. Corrected results for prompt $\psi(2S)$ and $\psi(2S)$ -from- b in the kinematic range $p_T(\psi(2S)) < 16$ GeV/ c and $2.0 < y(\psi(2S)) < 4.5$ are

$$\begin{aligned}\sigma_{\text{prompt}}(\psi(2S)) &= 1.37 \pm 0.01 \text{ (stat)} \pm 0.06 \text{ (syst)}_{-0.38}^{+0.19} \text{ (pol)} \text{ } \mu\text{b}, \\ \sigma_b(\psi(2S)) &= 0.31 \pm 0.01 \text{ (stat)} \pm 0.02 \text{ (syst)} \text{ } \mu\text{b}.\end{aligned}$$

where the last uncertainty on the prompt cross-section is due to the unknown $\psi(2S)$ polarization. With the corrected $\psi(2S)$ -from- b cross-section the inclusive branching fraction is updated by

$$\mathcal{B}(b \rightarrow \psi(2S)X) = (3.08 \pm 0.07(\text{stat}) \pm 0.36(\text{syst}) \pm 0.27(\mathcal{B})) \times 10^{-3}.$$

A.1 Nature of the correction

In Ref. [1], the production rate of $\psi(2S)$ mesons in the rapidity range $2.0 < y < 4.5$ was measured for pp collisions at $\sqrt{s} = 7$ TeV using a sample of data corresponding to 36 pb^{-1} . Both overall and singly differential ($d\sigma/dp_T$) cross-sections were measured by fitting the invariant-mass spectra to obtain background-subtracted signal yields, which are subsequently efficiency corrected. Two decay modes were used: $\psi(2S) \rightarrow \mu^+\mu^-$ and $\psi(2S) \rightarrow J/\psi(\mu^+\mu^-)\pi^+\pi^-$.

Two sources of $\psi(2S)$ production are expected in this environment: mesons produced promptly in the primary interaction (whether directly or through the decay of an intermediate resonance), and those produced via the decays of b hadrons. The vast majority of b hadrons produced in the LHCb acceptance consist of B^0 , B^+ , B_s^0 mesons and Λ_b^0 baryons, all with mean lifetimes of approximately 1.5 ps. Consequently, the two classes of production may be separated according to whether the $\psi(2S)$ originates from the primary vertex (PV) or from a downstream secondary vertex. This separation must be done on a statistical level, since some b hadrons will decay close to the PV on the scale of the experimental resolution.

The pseudo-decay-time t_z was used to distinguish the two sources of production, and is defined as

$$t_z = \frac{(z_{\psi(2S)} - z_{\text{PV}}) \times M_{\psi(2S)}}{p_z}, \quad (1)$$

where $z_{\psi(2S)}$ and z_{PV} are the z coordinates of the reconstructed $\psi(2S)$ decay vertex and the primary vertex, p_z is the z -component of the measured $\psi(2S)$ momentum, $M_{\psi(2S)}$ is the known $\psi(2S)$ mass [2], and the z -axis is the direction of the proton beam pointing downstream into the LHCb acceptance. For a given sample of $\psi(2S)$ candidates, a fit to the t_z distribution was used to obtain the prompt fraction f_p , as described in Sec. 4 of Ref. [1].

Two distinct problems related to the determination of f_p in Ref. [1] have been identified. The first is that a mathematical mistake was made in calculating the systematic uncertainties on the from- b $\psi(2S)$ production cross-sections that arise due to uncertainties

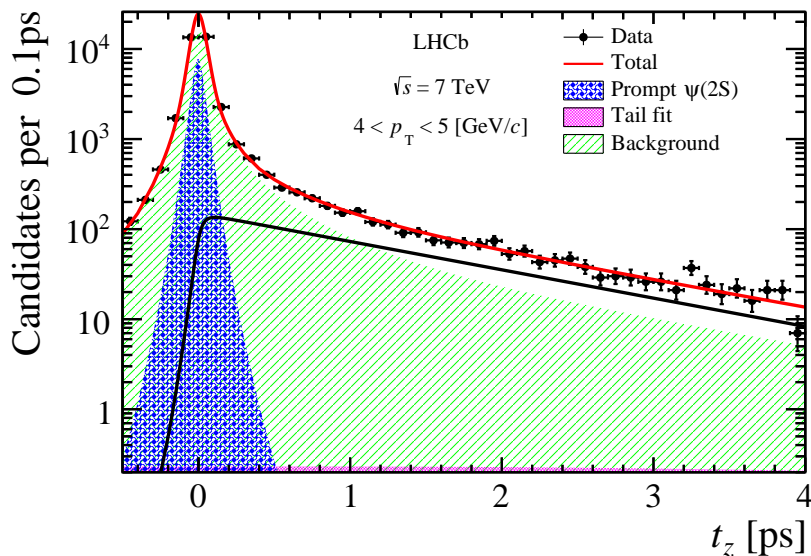


Figure 3: Pseudo-decay-time t_z distribution for the $\psi(2S) \rightarrow \mu^+\mu^-$ decay mode in the range $4 < p_T \leq 5$ GeV/c, showing the background and prompt contributions.

in the t_z fit; a factor of $f_p/(1 - f_p)$ was omitted. When this mistake is corrected, those systematic uncertainties increase by a factor 3 to 9, depending on the p_T defined in the range $0 - 16$ GeV/c, with the largest effect at low p_T , where the prompt fraction is close to unity. The correct formula is used in the results below.

The second problem is related to the values of f_p themselves. A mistake appears to have been made in the measurement of f_p via the fits to the t_z distributions used in Ref. [1]. An independent reimplementation of the analysis finds consistently lower values of f_p . This change in f_p is associated with a change in the mean value of t_z seen for the from- b component: values of approximately 1.1 ps were found in the analysis reported in Ref. [1], compared to approximately 1.5 ps (much closer to the mean lifetime of contributing b hadrons) in the reimplementation. This issue has been found using both the original t_z fit function as described in Ref. [1] and the function used in Ref. [3]. The more sophisticated t_z fit function used in Ref. [3] achieves a more precise description of experimental data and is thus used in obtaining corrections as described below. An example of a t_z fit in the p_T range $4 < p_T \leq 5$ GeV/c is shown in Fig. 3.

Because the issue found is limited to the determination of f_p and does not affect the combined cross-section, and given that the reimplementation uses a sample of $\psi(2S) \rightarrow \mu^+\mu^-$ events that is correlated with but not identical to the original analysis, the approach used in this erratum is to use the new and old values of f_p to determine a correction factor to apply to the results of the prompt and from- b cross-sections of the original analysis. (A separate and statistically independent analysis of the larger 7 TeV data sample taken in 2011 has been submitted [3] but is outside the scope of this erratum.) Defining $f_b \equiv 1 - f_p$ for convenience, the ratio

$$\mathcal{R}_b = \frac{f_b \text{ obtained with reimplementation}}{f_b(\psi(2S) \rightarrow \mu^+\mu^-) \text{ obtained in original analysis}} \quad (2)$$

is determined in bins of p_T . The correction is then obtained by fitting a linear function to the individual values of R_b . This also allows the correction to be extrapolated to kinematic regions where data were not available for the reimplementation ($p_T < 2 \text{ GeV}/c$, $p_T > 11 \text{ GeV}/c$). This correction is applied to the weighted average of $\psi(2S) \rightarrow \mu^+\mu^-$ and $\psi(2S) \rightarrow J/\psi(\mu^+\mu^-)\pi^+\pi^-$ results as reported by Ref. [1].

After applying the correction to f_b , the systematic uncertainties are recomputed. These are unchanged respect to those of the original analysis (other than relative uncertainties being updated for the new central values) except as described below. First, the the mistake in the computation of the uncertainty associated with the t_z fit is corrected as described above. Second, a new systematic uncertainty associated with the f_b correction estimate is added, and in particular the extrapolation outside the fit region, which is determined by taking the difference between the correction fitted by a first-order and a second-order polynomial.

A.2 Corrected results

The impact on f_p itself and on the cross-section for prompt production is modest: they are both reduced by an amount typically of the order of several percent. However the relative impact on f_b is greater, and the from- b cross-section rises by typically 20–25%.

Corrected versions of all figures and tables in Ref. [1] that were affected by the issue are given in the following. The corrected f_p distribution as a function of p_T is shown in Fig. 4. The singly differential cross-section as a function of p_T is shown for prompt production in Fig. 7, and for production from b -hadrons in Fig. 8. In the figures, the updated cross-sections are compared with theory predictions, namely NRQCD calculations [4] for prompt production and FONLL calculations [5] for production of $\psi(2S)$ from b -hadron decays. The integrated cross-sections in the nominal kinematic range for prompt $\psi(2S)$ and $\psi(2S)$ -from- b are found to be

$$\begin{aligned}\sigma_{\text{prompt}}(\psi(2S)) &= 1.37 \pm 0.01 \text{ (stat)} \pm 0.06 \text{ (syst)}_{-0.38}^{+0.19} \text{ (pol)} \mu\text{b}, \\ \sigma_b(\psi(2S)) &= 0.31 \pm 0.01 \text{ (stat)} \pm 0.02 \text{ (syst)} \mu\text{b}.\end{aligned}$$

The numerical results are given in Table 2.

Corrected ratio of $\psi(2S) \rightarrow \mu^+\mu^-$ and $J/\psi \rightarrow \mu^+\mu^-$ cross-sections for prompt production (R_p) and for b -hadron decay (R_b) as a function of p_T is shown on Fig. 9.

The inclusive $b \rightarrow \psi(2S)X$ branching fraction is computed using the $\psi(2S)$ -from- b cross-sections reported above and found to be

$$\mathcal{B}(b \rightarrow \psi(2S)X) = (3.08 \pm 0.07(\text{stat}) \pm 0.36(\text{syst}) \pm 0.27(\mathcal{B})) \times 10^{-3}.$$

The last uncertainty is due to those of the branching fractions, and is dominated by the $\mathcal{B}(b \rightarrow J/\psi X)$ uncertainty.

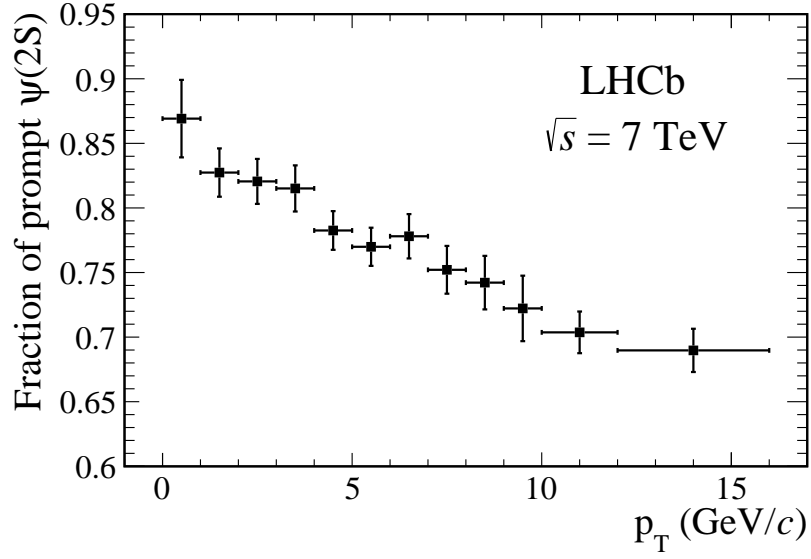


Figure 4: Fraction of prompt $\psi(2S)$, f_p , as a function of p_T . The error bars include statistical and systematic uncertainties added in quadrature.

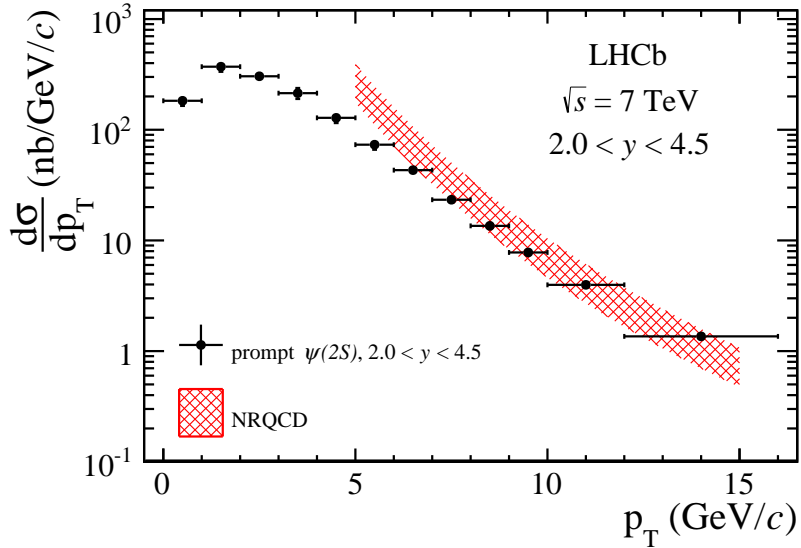


Figure 7: Differential production cross-section of prompt $\psi(2S)$ as a function of p_T in the range $2.0 < y < 4.5$. The results are compared with the NRQCD calculations [4]. The error bars include statistical and systematic uncertainties added in quadrature.

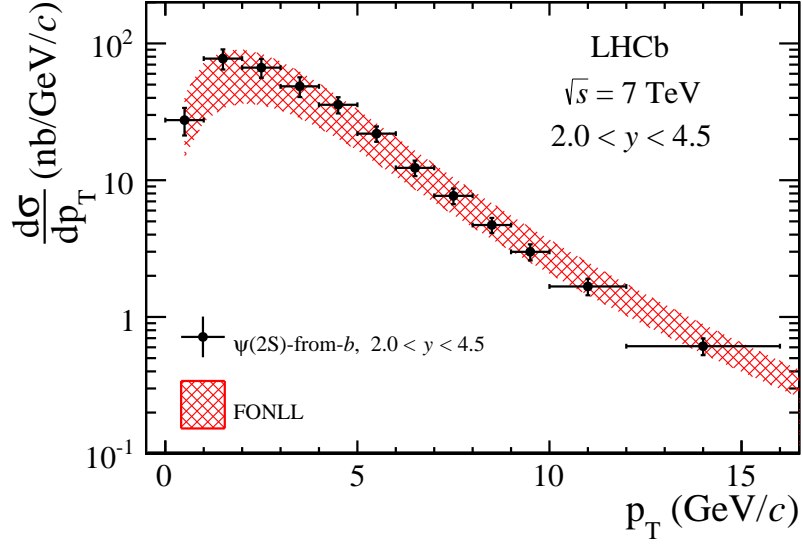


Figure 8: Differential production cross-section of $\psi(2S)$ from b hadrons as a function of p_T in the range $2.0 < y < 4.5$. The results are compared with the FONLL calculations [5]. The error bars include statistical and systematic uncertainties added in quadrature.

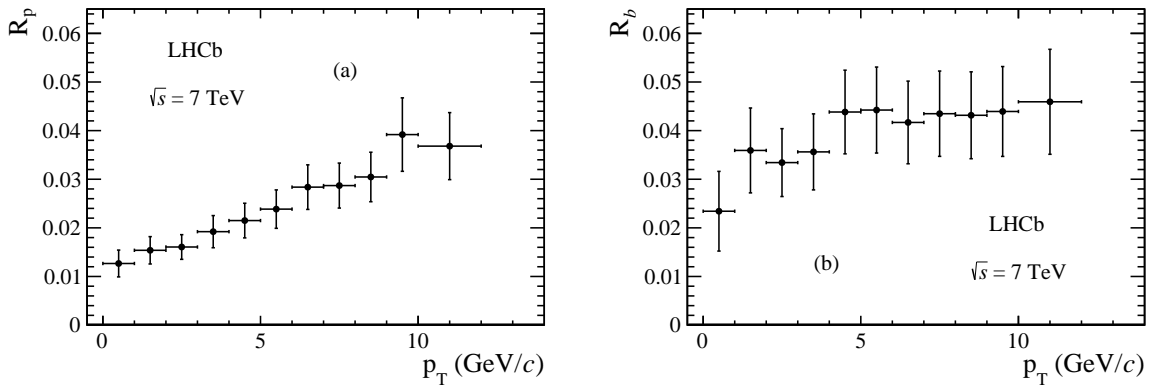


Figure 9: Ratio of $\psi(2S) \rightarrow \mu^+\mu^-$ and $J/\psi \rightarrow \mu^+\mu^-$ cross-sections for prompt production (a) and for b -hadron decay (b), as a function of p_T .

Table 2: Differential cross-sections $d\sigma/dp_T$ (in $\text{nb}/(\text{GeV}/c)$) of prompt $\psi(2S)$ and $\psi(2S)$ -from- b hadrons at $\sqrt{s} = 7 \text{ TeV}$, integrated over y between 2.0 and 4.5. The first uncertainty is statistical and the second systematic. The third asymmetric uncertainty for the prompt $\psi(2S)$ mesons is due to the unknown polarisation.

p_T (GeV/ c)	Prompt $\psi(2S)$	$\psi(2S)$ -from- b
0–1	$183 \pm 6 \pm 18 \begin{smallmatrix} +31 \\ -65 \end{smallmatrix}$	$28 \pm 3 \pm 6$
1–2	$371 \pm 7 \pm 37 \begin{smallmatrix} +58 \\ -114 \end{smallmatrix}$	$77 \pm 4 \pm 13$
2–3	$304 \pm 6 \pm 26 \begin{smallmatrix} +42 \\ -84 \end{smallmatrix}$	$67 \pm 3 \pm 10$
3–4	$214 \pm 6 \pm 24 \begin{smallmatrix} +26 \\ -51 \end{smallmatrix}$	$49 \pm 3 \pm 8$
4–5	$128 \pm 4 \pm 13 \begin{smallmatrix} +15 \\ -29 \end{smallmatrix}$	$36 \pm 2 \pm 4$
5–6	$73 \pm 2 \pm 7 \begin{smallmatrix} +9 \\ -17 \end{smallmatrix}$	$22 \pm 1 \pm 3$
6–7	$43 \pm 1 \pm 4 \begin{smallmatrix} +5 \\ -9 \end{smallmatrix}$	$12 \pm 1 \pm 1$
7–8	$23 \pm 1 \pm 2 \begin{smallmatrix} +3 \\ -6 \end{smallmatrix}$	$7.7 \pm 0.5 \pm 0.9$
8–9	$14 \pm 1 \pm 1 \begin{smallmatrix} +2 \\ -3 \end{smallmatrix}$	$4.7 \pm 0.3 \pm 0.5$
9–10	$7.8 \pm 0.4 \pm 0.7 \begin{smallmatrix} +0.8 \\ -1.6 \end{smallmatrix}$	$3.0 \pm 0.3 \pm 0.3$
10–12	$4.0 \pm 0.2 \pm 0.4 \begin{smallmatrix} +0.5 \\ -0.7 \end{smallmatrix}$	$1.7 \pm 0.2 \pm 0.2$
12–16	$1.4 \pm 0.1 \pm 0.2 \begin{smallmatrix} +0.2 \\ -0.3 \end{smallmatrix}$	$0.61 \pm 0.05 \pm 0.07$
0–16	$1366 \pm 13 \pm 56 \begin{smallmatrix} +190 \\ -380 \end{smallmatrix}$	$308 \pm 6 \pm 19$

References

- [1] LHCb collaboration, R. Aaij *et al.*, *Measurement of $\psi(2S)$ meson production in pp collisions at $\sqrt{s} = 7$ TeV*, Eur. Phys. J. **C72** (2012) 2100, [arXiv:1204.1258](#).
- [2] Particle Data Group, J. Beringer *et al.*, *Review of particle physics*, Phys. Rev. **D86** (2012) 010001, and 2013 partial update for the 2014 edition.
- [3] LHCb collaboration, R. Aaij *et al.*, *Measurement of $\psi(2S)$ production cross-sections in proton-proton collisions at $\sqrt{s} = 7$ and 13 TeV*, Eur. Phys. J. **C80** (2019) 2100, [arXiv:1908.03099](#).
- [4] H.-S. Shao *et al.*, *Yields and polarizations of prompt J/ψ and $\psi(2S)$ production in hadronic collisions*, JHEP **05** (2015) 103, [arXiv:1411.3300](#).
- [5] M. Cacciari, M. Greco, and P. Nason, *The p_T spectrum in heavy-flavour hadroproduction*, JHEP **05** (1998) 007, [arXiv:hep-ph/9803400](#).

LHCb collaboration

R. Aaij²³, C. Abellán Beteta³⁵, B. Adeva³⁶, M. Adinolfi⁴³, C. Adrover⁶, A. Affolder⁴⁹,
 Z. Ajaltouni⁵, J. Albrecht³⁷, F. Alessio³⁷, M. Alexander⁴⁸, G. Alkhazov²⁹, P. Alvarez Cartelle³⁶,
 A.A. Alves Jr²², S. Amato², Y. Amhis³⁸, J. Anderson³⁹, F. Andrianala³⁷, R.B. Appleby⁵¹,
 F. Archilli^{17,37}, L. Arrabito⁵⁵, A. Artamonov³⁴, M. Artuso^{53,37}, E. Aslanides⁶, G. Auriemma^{22,l},
 S. Bachmann¹¹, J.J. Back⁴⁵, D.S. Bailey⁵¹, V. Balagura^{30,37}, W. Baldini¹⁵, R.J. Barlow⁵¹,
 C. Barschel³⁷, S. Barsuk⁷, W. Barter⁴⁴, A. Bates⁴⁸, Th. Bauer²³, A. Bay³⁸, I. Bediaga¹,
 S. Belogurov³⁰, K. Belous³⁴, I. Belyaev^{30,37}, E. Ben-Haim⁸, M. Benayoun⁸, G. Bencivenni¹⁷,
 S. Benson⁴⁷, J. Benton⁴³, R. Bernet³⁹, M.O. Bettler¹⁶, M. van Beuzekom²³, A. Bien¹¹,
 S. Bifani¹², A. Bizzeti^{16,m}, P.M. Bjørnstad⁵¹, T. Blake³⁷, F. Blanc³⁸, C. Blanks⁵⁰, J. Blouw¹¹,
 S. Blusk⁵³, A. Bobrov³³, V. Bocci²², A. Bondar^{33,n}, N. Bondar²⁹, W. Bonivento²⁰, S. Borghi⁴⁸,
 A. Borgia⁵³, T.J.V. Bowcock⁴⁹, C. Bozzi¹⁵, T. Brambach⁹, J. van den Brand²⁴, J. Bressieux³⁸,
 D. Brett⁵¹, M. Britsch¹⁰, T. Britton⁵³, N.H. Brook⁴³, H. Brown⁴⁹, A. Bursche³⁹, J. Buytaert³⁷,
 A. Büchler-Germann³⁹, S. Cadeddu²⁰, O. Callot⁷, M. Calvi^{19,f}, M. Calvo Gomez^{35,i},
 A. Camboni³⁵, P. Campana^{17,37}, A. Carbone^{14,c}, G. Carboni^{21,g}, R. Cardinale^{18,37}, A. Cardini²⁰,
 L. Carson⁵⁰, K. Carvalho Akiba², G. Casse⁴⁹, M. Cattaneo³⁷, Ch. Cauet⁹, M. Charles⁵²,
 Ph. Charpentier³⁷, N. Chiapolini³⁹, M. Chrzaszcz²⁵, P. Ciambrone¹⁷, K. Ciba³⁷, X. Cid Vidal³⁶,
 G. Ciezarek⁵⁰, P.E.L. Clarke^{47,37}, M. Clemencic³⁷, H.V. Cliff⁴⁴, J. Closier³⁷, C. Coca²⁸,
 V. Coco²³, J. Cogan⁶, P. Collins³⁷, A. Comerma-Montells³⁵, F. Constantin²⁸, A. Cook⁴³,
 M. Coombes⁴³, G. Corti³⁷, B. Couturier³⁷, G.A. Cowan³⁸, R. Currie⁴⁷, C. D'Ambrosio³⁷,
 P. David⁸, P.N.Y. David²³, O. De Aguiar Francisco², K. De Bruyn²³, M. De Cian³⁹,
 F. De Lorenzi¹², J.M. De Miranda¹, L. De Paula², P. De Simone¹⁷, D. Decamp⁴, M. Deckenhoff⁹,
 H. Degaudenzi^{38,37}, L. Del Buono⁸, C. Deplano²⁰, D. Derkach^{14,37}, O. Deschamps⁵, F. Dettori²⁴,
 J. Dickens⁴⁴, H. Dijkstra³⁷, P. Diniz Batista¹, F. Domingo Bonal³⁵, S. Donleavy⁴⁹, F. Dordei¹¹,
 A. Dosil Suárez³⁶, D. Dossett⁴⁵, A. Dovbnya⁴⁰, F. Dupertuis³⁸, R. Dzhelyadin³⁴, A. Dziurda²⁵,
 S. Easo⁴⁶, U. Egede⁵⁰, V. Egorychev³⁰, S. Eidelman^{33,n}, D. van Eijk²³, F. Eisele¹¹,
 S. Eisenhardt⁴⁷, R. Ekelhof⁹, L. Eklund^{48,37}, Ch. Elsasser³⁹, D. Elsby⁴², D. Esperante Pereira³⁶,
 A. Falabella¹⁴, E. Fanchini¹⁹, G. Fardell⁴⁷, C. Farinelli²³, S. Farry¹², V. Fave³⁸,
 V. Fernandez Albor³⁶, F. Ferreira Rodrigues¹, M. Ferro-Luzzi³⁷, S. Filippov³², C. Fitzpatrick⁴⁷,
 M. Fontana¹⁰, F. Fontanelli^{18,e}, R. Forty³⁷, M. Frank³⁷, C. Frei³⁷, M. Frosini^{16,37}, S. Furcas¹⁹,
 C. Färber¹¹, A. Gallas Torreira³⁶, D. Galli^{14,c}, M. Gandelman², P. Gandini⁵², Y. Gao³,
 J-C. Garnier³⁷, J. Garofoli⁵³, J. Garra Tico⁴⁴, L. Garrido³⁵, D. Gascon³⁵, C. Gaspar³⁷,
 R. Gauld⁵², N. Gauvin³⁸, M. Gersabeck³⁷, T. Gershon^{45,37}, Ph. Ghez⁴, V. Gibson⁴⁴,
 V.V. Gligorov³⁷, D. Golubkov³⁰, A. Golutvin^{50,30,37}, A. Gomes², H. Gordon⁵², C. Gotti^{19,f},
 M. Grabalosa Gándara³⁵, R. Graciani Diaz³⁵, L.A. Granado Cardoso³⁷, E. Graugés³⁵,
 G. Graziani¹⁶, A. Greco²⁸, E. Greening⁵², S. Gregson⁴⁴, B. Gui⁵³, E. Gushchin³², Yu. Guz³⁴,
 T. Gys³⁷, C. Göbel⁵⁴, C. Hadjivasiliou⁵³, G. Haefeli³⁸, C. Haen³⁷, S.C. Haines⁴⁴, T. Hampson⁴³,
 S. Hansmann-Menzemer¹¹, R. Harji⁵⁰, N. Harnew⁵², J. Harrison⁵¹, P.F. Harrison⁴⁵,
 T. Hartmann⁵⁶, J. He⁷, V. Heijne²³, K. Hennessy⁴⁹, P. Henrard⁵, J.A. Hernando Morata³⁶,
 E. van Herwijnen³⁷, E. Hicks⁴⁹, K. Holubyev¹¹, W. Hulsbergen²³, P. Hunt⁵², T. Huse⁴⁹,
 R.S. Huston¹², D. Hutchcroft⁴⁹, D. Hynds⁴⁸, V. Iakovenko⁴¹, P. Ilten¹², J. Imong⁴³,
 A. Inyakin³⁴, R. Jacobsson³⁷, A. Jaeger¹¹, M. Jahjah Hussein⁵, E. Jans²³, F. Jansen²³,
 P. Jaton³⁸, B. Jean-Marie⁷, F. Jing³, M. John⁵², D. Johnson⁵², C.R. Jones⁴⁴, B. Jost³⁷,
 S. Kandybei⁴⁰, M. Karacson³⁷, T.M. Karbach⁹, J. Keaveney¹², I.R. Kenyon⁴², U. Kerzel³⁷,
 T. Ketel²⁴, A. Keune³⁸, B. Khanji⁶, Y.M. Kim⁴⁷, M. Knecht³⁸, R.F. Koopman²⁴,
 P. Koppenburg²³, A. Kozlinskiy²³, L. Kravchuk³², K. Kreplin¹¹, M. Kreps⁴⁵, G. Krocker¹¹,
 P. Krokovny^{33,n}, F. Kruse⁹, K. Kruzelecki³⁷, M. Kucharczyk^{19,37}, T. Kvaratskheliya^{30,37},
 V.N. La Thi³⁸, D. Lacarrere³⁷, G. Lafferty⁵¹, A. Lai²⁰, D. Lambert⁴⁷, R.W. Lambert²⁴,
 E. Lanciotti³⁷, G. Lanfranchi¹⁷, C. Langenbruch¹¹, T. Latham⁴⁵, C. Lazzeroni⁴², R. Le Gac⁶,

J. van Leerdam²³, J.-P. Lees⁴, A. Leflat^{31,37}, J. Lefrançois⁷, R. Lefèvre⁵, O. Leroy⁶, T. Lesiak²⁵, L. Li³, P.-R. Li^{57,o}, L. Li Gioi⁵, M. Lieng⁹, M. Liles⁴⁹, R. Lindner³⁷, C. Linn¹¹, B. Liu³, G. Liu³⁷, J. von Loeben¹⁹, J.H. Lopes², E. Lopez Asamar³⁵, N. Lopez-March³⁸, H. Lu³, J. Luisier³⁸, X. Lyu⁵⁷, A. Mac Raighne⁴⁸, F. Machefer⁷, F. Maciuc¹⁰, O. Maev^{29,37}, S. Malde⁵², R.M.D. Mamunur³⁷, G. Manca²⁰, G. Mancinelli⁶, N. Mangiafave⁴⁴, J.F. Marchand⁴, U. Marconi¹⁴, J. Marks¹¹, G. Martellotti²², A. Martens⁸, L. Martin⁵², D. Martinez Santos³⁷, A. Martín Sánchez⁷, A. Massafferri¹, Z. Mathe¹², C. Matteuzzi¹⁹, M. Matveev²⁹, E. Maurice⁶, B. Maynard⁵³, A. Mazurov^{15,32,37}, G. McGregor⁵¹, R. McNulty¹², M. Meissner¹¹, M. Merk²³, J. Merkel⁹, R. Messi²¹, S. Miglioranzi³⁷, D.A. Milanese^{13,37}, M.-N. Minard⁴, J. Molina Rodriguez⁵⁴, S. Monteil⁵, D. Moran¹², P. Morawski²⁵, R. Mountain⁵³, I. Mous²³, F. Muheim⁴⁷, R. Muresan^{38,28}, B. Muster³⁸, M. Musy³⁵, J. Mylroie-Smith⁴⁹, R. Märki³⁸, K. Müller³⁹, P. Naik⁴³, T. Nakada³⁸, R. Nandakumar⁴⁶, I. Nasteva¹, M. Nedos⁹, M. Needham⁴⁷, N. Neufeld³⁷, A.D. Nguyen³⁸, C. Nguyen-Mau^{38,j}, M. Nicol⁷, V. Niess⁵, N. Nikitin³¹, T. Nikodem¹¹, A. Nomerotski^{52,37}, A. Novoselov³⁴, A. Oblakowska-Mucha²⁶, V. Obraztsov³⁴, S. Oggero²³, S. Ogilvy⁴⁸, R. Oldeman²⁰, J.M. Otalora Goicochea², P. Owen⁵⁰, B.K. Pal⁵³, J. Palacios³⁹, A. Palano^{13,b}, M. Palutan¹⁷, J. Panman³⁷, A. Papanestis⁴⁶, M. Pappagallo⁴⁸, C. Parkes^{51,37}, C.J. Parkinson⁵⁰, G. Passaleva¹⁶, G.D. Patel⁴⁹, M. Patel⁵⁰, S.K. Paterson⁵⁰, G.N. Patrick⁴⁶, C. Patrignani^{18,e}, A. Pellegrino²³, G. Penso^{22,h}, M. Pepe Altarelli³⁷, S. Perazzini^{14,c}, D.L. Perego¹⁹, P. Perret⁵, M. Perrin-Terrin⁶, A. Petrella¹⁵, A. Petrolini^{18,e}, A. Phan⁵³, E. Picatoste Olloqui³⁵, B. Pie Valls³⁵, B. Pietrzyk⁴, T. Pilar⁴⁵, D. Pinci²², R. Plackett⁴⁸, S. Playfer⁴⁷, M. Plo Casasus³⁶, G. Polok²⁵, A. Poluektov^{45,33}, I. Polyakov³⁰, E. Polcarpo², D. Popov¹⁰, B. Popovici²⁸, C. Potterat³⁵, A. Powell^{52,45}, J. Prisciandaro³⁸, V. Pugatch⁴¹, A. Puig Navarro³⁵, A. Pérez-Calero Yzquierdo³⁵, W. Qian⁵³, J.H. Rademacker⁴³, B. Rakotomiamanana³⁸, M.S. Rangel², I. Raniuk⁴⁰, G. Raven²⁴, S. Redford⁵², M.M. Reid⁴⁵, A.C. dos Reis¹, S. Ricciardi⁴⁶, A. Richards⁵⁰, K. Rinnert⁴⁹, D.A. Roa Romero⁵, P. Robbe⁷, E. Rodrigues^{48,51}, P. Rodriguez Perez³⁶, G.J. Rogers⁴⁴, S. Roiser³⁷, V. Romanovskiy³⁴, J. Rouvinet³⁸, T. Ruf³⁷, H. Ruiz³⁵, G. Sabatino²¹, J.J. Saborido Silva³⁶, N. Sagidova²⁹, P. Sail⁴⁸, B. Saitta^{20,d}, C. Salzmann³⁹, M. Sannino¹⁸, R. Santacesaria²², C. Santamarina Rios³⁶, R. Santinelli³⁷, E. Santovetti^{21,g}, M. Sapunov⁶, A. Sarti¹⁷, C. Satriano^{22,l}, A. Satta²¹, M. Saur⁵⁷, D. Savrina^{30,31}, P. Schaack⁵⁰, M. Schiller²⁴, S. Schleich⁹, M. Schlupp⁹, M. Schmelling¹⁰, B. Schmidt³⁷, O. Schneider³⁸, A. Schopper³⁷, M.H. Schune⁷, R. Schwemmer³⁷, B. Sciascia¹⁷, A. Sciubba¹⁷, A. Semennikov³⁰, K. Senderowska²⁶, I. Sepp⁵⁰, N. Serra³⁹, J. Serrano⁶, P. Seyfert¹¹, M. Shapkin³⁴, Y. Shcheglov²⁹, T. Shears⁴⁹, L. Shekhtman^{33,n}, V. Shevchenko³⁰, A. Shires⁵⁰, R. Silva Coutinho⁴⁵, T. Skwarnicki⁵³, E. Smith^{52,46}, K. Sobczak⁵, F.J.P. Soler⁴⁸, A. Solomin⁴³, F. Soomro¹⁷, B. Souza De Paula², B. Spaan⁹, A. Sparkes⁴⁷, P. Spradlin⁴⁸, F. Stagni³⁷, S. Stahl¹¹, O. Steinkamp³⁹, O. Stenyakin³⁴, S. Stoica²⁸, S. Stone^{53,37}, B. Storaci²³, M. Straticiu²⁸, U. Straumann³⁹, V.K. Subbiah³⁷, S. Swientek⁹, M. Szczekowski²⁷, P. Szczypka^{38,37}, T. Szumlak²⁶, S. T'Jampens⁴, E. Teodorescu²⁸, F. Teubert³⁷, E. Thomas³⁷, J. van Tilburg¹¹, V. Tisserand⁴, M. Tobin³⁹, N. Torr⁵², E. Tournefier^{4,50}, S. Tourneur³⁸, M.T. Tran³⁸, A. Tsaregorodtsev⁶, N. Tuning²³, M. Ubeda Garcia³⁷, A. Ukleja²⁷, P. Urquijo⁵³, U. Uwer¹¹, V. Vagnoni¹⁴, G. Valenti¹⁴, R. Vazquez Gomez³⁵, P. Vazquez Regueiro³⁶, S. Vecchi¹⁵, J.J. Velthuis⁴³, M. Veltri^{16,k}, B. Viaud⁷, I. Videau⁷, D. Vieira², X. Vilasis-Cardona^{35,i}, J. Visniakov³⁶, A. Vollhardt³⁹, D. Volyanskyy¹⁰, D. Voong⁴³, A. Vorobyev²⁹, S. Wandernoth¹¹, J. Wang⁵³, D.R. Ward⁴⁴, N.K. Watson⁴², A.D. Webber⁵¹, D. Websdale⁵⁰, M. Whitehead⁴⁵, D. Wiedner¹¹, L. Wiggers²³, G. Wilkinson⁵², M.P. Williams^{45,46}, M. Williams⁵⁰, F.F. Wilson⁴⁶, J. Wishahi⁹, M. Witek²⁵, W. Witzeling³⁷, S.A. Wotton⁴⁴, K. Wyllie³⁷, Y. Xie⁴⁷, Z. Xing⁵³, Z. Yang³, R. Young⁴⁷, O. Yushchenko³⁴, M. Zangoli¹⁴, M. Zavertyaev^{10,a}, F. Zhang³, L. Zhang⁵³, W.C. Zhang¹², Y. Zhang³, A. Zhelezov¹¹, A. Zhokhov³⁰, L. Zhong³, A. Zvyagin³⁷.

¹Centro Brasileiro de Pesquisas Físicas (CBPF), Rio de Janeiro, Brazil

- ² *Universidade Federal do Rio de Janeiro (UFRJ), Rio de Janeiro, Brazil*
- ³ *Center for High Energy Physics, Tsinghua University, Beijing, China*
- ⁴ *Univ. Grenoble Alpes, Univ. Savoie Mont Blanc, CNRS, IN2P3-LAPP, Annecy, France*
- ⁵ *Université Clermont Auvergne, CNRS/IN2P3, LPC, Clermont-Ferrand, France*
- ⁶ *Aix Marseille Univ, CNRS/IN2P3, CPPM, Marseille, France*
- ⁷ *LAL, Univ. Paris-Sud, CNRS/IN2P3, Université Paris-Saclay, Orsay, France*
- ⁸ *LPNHE, Sorbonne Université, Paris Diderot Sorbonne Paris Cité, CNRS/IN2P3, Paris, France*
- ⁹ *Fakultät Physik, Technische Universität Dortmund, Dortmund, Germany*
- ¹⁰ *Max-Planck-Institut für Kernphysik (MPIK), Heidelberg, Germany*
- ¹¹ *Physikalisches Institut, Ruprecht-Karls-Universität Heidelberg, Heidelberg, Germany*
- ¹² *School of Physics, University College Dublin, Dublin, Ireland*
- ¹³ *INFN Sezione di Bari, Bari, Italy*
- ¹⁴ *INFN Sezione di Bologna, Bologna, Italy*
- ¹⁵ *INFN Sezione di Ferrara, Ferrara, Italy*
- ¹⁶ *INFN Sezione di Firenze, Firenze, Italy*
- ¹⁷ *INFN Laboratori Nazionali di Frascati, Frascati, Italy*
- ¹⁸ *INFN Sezione di Genova, Genova, Italy*
- ¹⁹ *INFN Sezione di Milano-Bicocca, Milano, Italy*
- ²⁰ *INFN Sezione di Cagliari, Monserrato, Italy*
- ²¹ *INFN Sezione di Roma Tor Vergata, Roma, Italy*
- ²² *INFN Sezione di Roma La Sapienza, Roma, Italy*
- ²³ *Nikhef National Institute for Subatomic Physics, Amsterdam, Netherlands*
- ²⁴ *Nikhef National Institute for Subatomic Physics and VU University Amsterdam, Amsterdam, Netherlands*
- ²⁵ *Henryk Niewodniczanski Institute of Nuclear Physics Polish Academy of Sciences, Kraków, Poland*
- ²⁶ *AGH - University of Science and Technology, Faculty of Physics and Applied Computer Science, Kraków, Poland*
- ²⁷ *National Center for Nuclear Research (NCBJ), Warsaw, Poland*
- ²⁸ *Horia Hulubei National Institute of Physics and Nuclear Engineering, Bucharest-Magurele, Romania*
- ²⁹ *Petersburg Nuclear Physics Institute NRC Kurchatov Institute (PNPI NRC KI), Gatchina, Russia*
- ³⁰ *Institute of Theoretical and Experimental Physics NRC Kurchatov Institute (ITEP NRC KI), Moscow, Russia, Moscow, Russia*
- ³¹ *Institute of Nuclear Physics, Moscow State University (SINP MSU), Moscow, Russia*
- ³² *Institute for Nuclear Research of the Russian Academy of Sciences (INR RAS), Moscow, Russia*
- ³³ *Budker Institute of Nuclear Physics (SB RAS), Novosibirsk, Russia*
- ³⁴ *Institute for High Energy Physics NRC Kurchatov Institute (IHEP NRC KI), Protvino, Russia, Protvino, Russia*
- ³⁵ *ICCUB, Universitat de Barcelona, Barcelona, Spain*
- ³⁶ *Instituto Galego de Física de Altas Enerxías (IGFAE), Universidade de Santiago de Compostela, Santiago de Compostela, Spain*
- ³⁷ *European Organization for Nuclear Research (CERN), Geneva, Switzerland*
- ³⁸ *Institute of Physics, Ecole Polytechnique Fédérale de Lausanne (EPFL), Lausanne, Switzerland*
- ³⁹ *Physik-Institut, Universität Zürich, Zürich, Switzerland*
- ⁴⁰ *NSC Kharkiv Institute of Physics and Technology (NSC KIPT), Kharkiv, Ukraine*
- ⁴¹ *Institute for Nuclear Research of the National Academy of Sciences (KINR), Kyiv, Ukraine*
- ⁴² *University of Birmingham, Birmingham, United Kingdom*
- ⁴³ *H.H. Wills Physics Laboratory, University of Bristol, Bristol, United Kingdom*
- ⁴⁴ *Cavendish Laboratory, University of Cambridge, Cambridge, United Kingdom*
- ⁴⁵ *Department of Physics, University of Warwick, Coventry, United Kingdom*
- ⁴⁶ *STFC Rutherford Appleton Laboratory, Didcot, United Kingdom*
- ⁴⁷ *School of Physics and Astronomy, University of Edinburgh, Edinburgh, United Kingdom*
- ⁴⁸ *School of Physics and Astronomy, University of Glasgow, Glasgow, United Kingdom*
- ⁴⁹ *Oliver Lodge Laboratory, University of Liverpool, Liverpool, United Kingdom*
- ⁵⁰ *Imperial College London, London, United Kingdom*
- ⁵¹ *School of Physics and Astronomy, University of Manchester, Manchester, United Kingdom*
- ⁵² *Department of Physics, University of Oxford, Oxford, United Kingdom*

⁵³ *Syracuse University, Syracuse, NY, United States*

⁵⁴ *Pontifícia Universidade Católica do Rio de Janeiro (PUC-Rio), Rio de Janeiro, Brazil, associated to ²*

⁵⁵ *CC-IN2P3, CNRS/IN2P3, Lyon-Villeurbanne, France, associated to ⁶*

⁵⁶ *Institut für Physik, Universität Rostock, Rostock, Germany, associated to ¹¹*

⁵⁷ *University of Chinese Academy of Sciences, Beijing, China, associated to ³*

^a *P.N. Lebedev Physical Institute, Russian Academy of Science (LPI RAS), Moscow, Russia*

^b *Università di Bari, Bari, Italy*

^c *Università di Bologna, Bologna, Italy*

^d *Università di Cagliari, Cagliari, Italy*

^e *Università di Genova, Genova, Italy*

^f *Università di Milano Bicocca, Milano, Italy*

^g *Università di Roma Tor Vergata, Roma, Italy*

^h *Università di Roma La Sapienza, Roma, Italy*

ⁱ *LIFAEELS, La Salle, Universitat Ramon Llull, Barcelona, Spain*

^j *Hanoi University of Science, Hanoi, Vietnam*

^k *Università di Urbino, Urbino, Italy*

^l *Università della Basilicata, Potenza, Italy*

^m *Università di Modena e Reggio Emilia, Modena, Italy*

ⁿ *Novosibirsk State University, Novosibirsk, Russia*

^o *Lanzhou University, Lanzhou, China*